



AUTOMATIC RESOLUTION CONTROL FOR THE FINITE-VOLUME METHOD, PART 3: TURBULENT FLOW APPLICATIONS

H. Jasak

Computational Dynamics Ltd., Hythe House, 200 Shepherds Bush Road, London W6 7NY, England

A. D. Gosman

Department of Mechanical Engineering, Imperial College of Science, Technology and Medicine, Exhibition Road, London SW7 2BX, England

The first two parts of this article [1, 2] describe the components of an automatic resolution control (ARC) algorithm for the finite-volume method. While the performance of similar algorithms is well established for inviscid supersonic flows and partly for laminar flows, the number of studies dealing with incompressible turbulent flows is very limited. In this article we shall apply the ARC to two turbulent flow test cases using the $k-\varepsilon$ turbulence model in 2- and 3-D to examine the performance of the method. For completeness, both the high-Re model with wall functions and the low-Re variant will be included.

1. INTRODUCTION

The popularity of adaptive mesh refinement in computational fluid dynamics (CFD) varies considerably across the field, depending on the physical properties of the flow under consideration. In supersonic flows with shocks, for example, mesh adaptivity is relatively widely used [3–10], while the number of adaptive solvers for incompressible [11–15] and particularly turbulent flows is very limited [16, 17].

This state of affairs can be partially explained based on the characteristics of the solution. In supersonic flows, regions of interest which require high mesh resolution have a dimensionality one less than that of the problem. In 3-D calculations, for example, mesh refinement is needed on 2-D shock surfaces; dealing with this in a localized manner is considerably cheaper than uniform refinement. The other extreme from the point of view of adaptive error control is a smooth solution in laminar flows, where mesh quality plays an important role in the overall discretization error.

Our main interest in this study is to examine the applicability of adaptive mesh algorithms to turbulent flows in a Reynolds-averaged framework. Here, the regions requiring high resolution are near the wall and in shear layers, with the additional

Received 24 January 2000; accepted 28 March 2000.

Address correspondence to Dr. Hrvoje Jasak, Computational Dynamics Ltd., Hythe House, 200 Shepherds Bush Road, London W6 7NY, England. E-mail: h.jasak@cd.co.uk

NOMENCLATURE

e	error in velocity	ε	dissipation of turbulent kinetic energy
k	turbulent kinetic energy		
Re	Reynolds number	λ_c	coarsening threshold
\mathbf{u}	velocity	λ_r	refinement threshold
y^+	dimensionless distance to the wall	ξ	alignment threshold

complication of complex and sometimes mesh-dependent mathematical models (e.g., wall functions [18]). For this purpose we shall apply the automatic resolution control (ARC) [2] on two representative test cases. As the “exact” error is not available, the results will be compared with uniform systematic refinement in terms of mesh quality and error reduction rate. Systematic refinement also allows us to examine the performance of error estimates from [1], both visually and in terms of error scaling.

The rest of the article is organized as follows. In Section 2, we shall examine a flow over a 2-D hill. In the first instance, laminar flow with $Re = 60$ will be simulated, giving us a possibility to validate the error estimates on a pressure–velocity system against an “exact numerical” solution obtained on a very fine mesh. In the second phase, turbulent flow is simulated with the ARC using both high-Re formulation (wall functions) and integration to the wall (low-Re model). A 3-D turbulent flow over a swept backward-facing step test case presented in Section 3 serves as an illustration of the behavior of the algorithm in three spatial dimensions. Here, we shall examine the efficiency of local refinement on a test case for which systematic uniform refinement is beyond the available computer resources. Finally, the observations on the performance of the ARC on turbulent flows are given in Section 4, and the article is briefly summarized.

All calculations were performed using the FOAM C++ CFD library [19], developed by H. G. Weller et al. in collaboration with the author. The FOAM pressure-based incompressible flow solver uses the generic second-order-accurate FVM discretization operators on arbitrarily unstructured meshes and implements a segregated solution procedure with a variant of PISO [20] pressure–velocity coupling. The Gamma differencing scheme [21] is used on all convection terms. FOAM offers a number of turbulence models (both RSTM and LES), and in this study we shall use the nonlinear version of the k – ε model by Shih et al. [22] with wall functions [18], unless otherwise stated.

2. FLOW OVER A 2-D HILL

The geometry of the test case consists of a symmetric hill in a tunnel, with a blockage ratio of hill height to channel depth of 1/6.07. Two flow regimes will be examined: laminar flow with $Re = 60$ and turbulent flow, $Re = 60,000$. Both flow regimes will be initially solved on four meshes created using transfinite mapping, with 518, 2,044, 8,584, and 34,336 CVs and slight grading toward the wall. In the second phase, the ARC will be used in two modes: refinement-only from a coarse

initial mesh, and refinement with coarsening from a finer mesh. For the laminar case, a parabolic inlet velocity profile will be used. The turbulent flow setup is identical to the ERCOFTAC code-comparison exercise [23, 24], which provides the inlet profiles for the velocity and turbulence quantities.

2.1 Laminar Flow

The accuracy of error estimates can be evaluated in absolute terms only if the exact solution for the problem is available. For laminar flows in 2-D it is reasonable to use a numerical solution from a very fine mesh in place of the analytical solution. For this purpose, the flow has been resolved on the mesh with 137,344 CVs and the solution has been mapped to other meshes. This “exact numerical” solution is of limited accuracy and is considered inappropriate to judge the accuracy of error estimation for meshes with more than 10,000 CVs.

As the role of the pressure equation is to enforce the continuity constraint on the velocity field, we shall concentrate on the velocity error, knowing that appropriate resolution of the velocity field implies accurate pressure distribution.

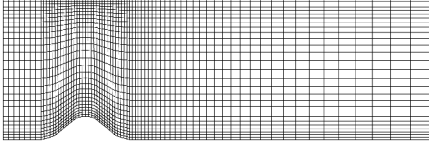
2.1.1. Systematic refinement. The solution obtained on the mesh with 2,044 CVs, as well as the “exact” and estimated errors, are shown in Figure 1.

The exact error $\mathbf{e} = \mathbf{u}_{\text{exact}} - \mathbf{u}_{\text{num}}$ has a vector form, each component giving the error in the corresponding velocity component. It is usually more informative to look at the magnitude of the exact error, Figure 1*d*. Here, three distinct parts of the error can be recognized. The first, upstream of the hill, is induced by the inlet boundary condition and spreads uniformly from the inlet boundary. For purposes of error analysis the boundary condition is considered exact; as a consequence, this error cannot be picked up by an error estimate. The second region of high error, caused by insufficient mesh resolution, envelops the hill, including the area just above the summit. The rest of the error is convected downstream from the peak. This is rapidly removed with mesh refinement and disappears on the next finer mesh.

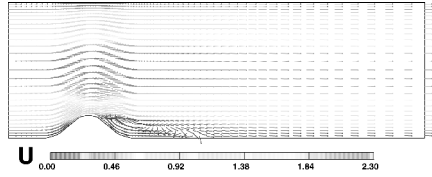
Both error estimates highlight the front of the hill as the region of high error sources, corresponding to the maximum error in Figure 1*d*. The recirculation zone behind the hill also induces some error, caused by the high local velocity gradients. The scaling of the exact error and the error estimates shows that the MEE captures the mean and maximum error with reasonable accuracy, particularly on coarse meshes. The Taylor series error estimate (TSEE) underpredicts the error magnitude, consistent with expectations.

2.1.2. Adaptive error control. In the second phase, the ARC will be used in two modes: refinement-only from the initial coarse mesh (2,044 CVs) and refinement with coarsening from the intermediate mesh (8,584 CVs). In both cases the MEE is used and the refinement parameters are set to $\lambda_r = 1.5$, $\lambda_c = 0.5$, and $\xi = 0.6$; the results are shown in Figure 2.

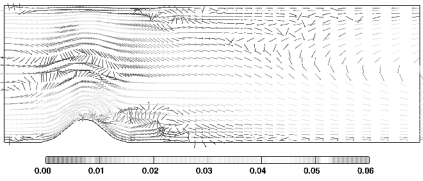
Mesh refinement concentrates the cells around the summit and in the recirculation region behind the hill. Some cells are also added close to the outlet boundary in the middle of the channel. Refinement with coarsening, Figure 2*b*, behaves in a similar way. The error reduction graph, Figure 2*d*, shows that in spite of the rapid



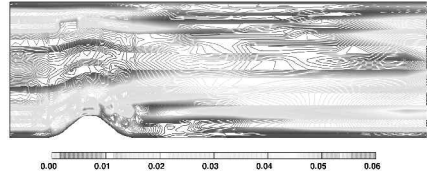
(a) Uniform coarse mesh, 2044 CVs.



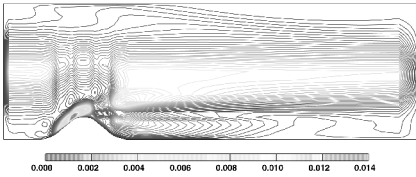
(b) Flow field.



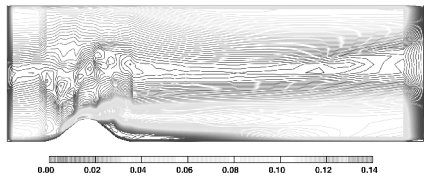
(c) Exact velocity error.



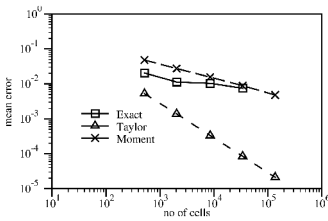
(d) Exact error magnitude.



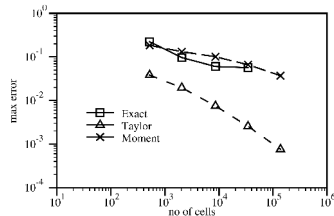
(e) Taylor series error estimate.



(f) Moment error estimate.

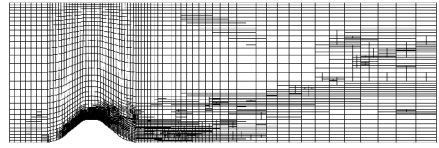
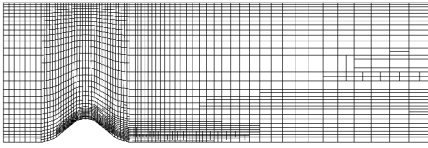


(g) Mean error.

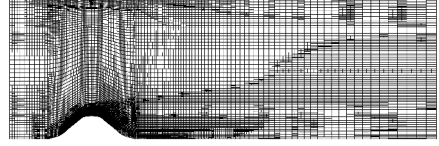
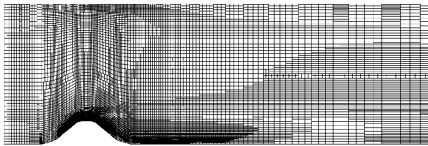


(h) Maximum error.

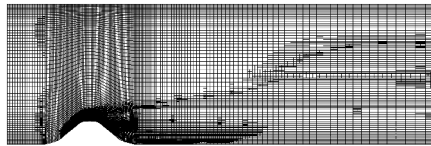
Figure 1. Laminar flow over a 2-D hill: systematic refinement. (a) Uniform coarse mesh, 2,044 CVs. (b) Flow field. (c) Exact velocity error. (d) Exact error magnitude. (e) Taylor series error estimate. (f) Moment error estimate. (g) Mean error. (h) Maximum error.



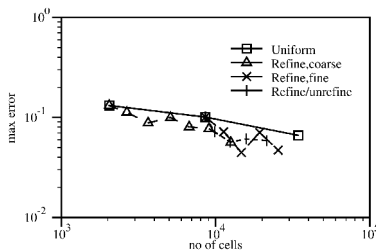
(a) Adaptive refinement.



(b) Refinement with coarsening.



(c) Refinement-only from the fine mesh.



(d) Maximum MEE for different refinement regimes.

Figure 2. Laminar flow over a 2-D hill: adaptive refinement. (a) Adaptive refinement. (b) Refinement with coarsening. (c) Refinement-only from the fine mesh. (d) Maximum MEE for different refinement regimes.

increase in local mesh resolution, improvements in accuracy are limited. The mesh quality is very important for adaptive laminar calculations, and the coarsening procedure introduces mesh distortions of such significance that its use cannot be justified. The adaptive procedure reduces the error marginally faster than uniform refinement according to the error estimates, with the best performance obtained from refinement-only from the intermediate mesh.

The error reduction does not change much if the TSEE is used to mark the cells for refinement; the largest change in the performance can be made by tuning λ_r , λ_c , and ξ , as they influence the quality of the refined mesh.

Overall, it can be concluded that laminar flows do not benefit much from local mesh adaptation. Here, the smoothness of the solution typically guarantees that even a coarse mesh will produce a result of reasonable accuracy. On the other hand, the mesh quality plays a major role in the overall discretization error, which is far from ideal for local mesh adaptation.

2.2 Turbulent Flow

The complexity of turbulent flows presents a considerably more challenging problem, both for error estimation and mesh adaptivity. Additional complications in error estimation are introduced by the wall treatment. When wall functions are used, the region of high gradients near the wall is bridged by a 1-D model, creating an additional term in the momentum equation to account for the increased wall shear stress. The additional drag can be treated as a change in the effective viscosity at the “wall face.” The rest of the model represents a highly nonlinear source term in the momentum equation, which cannot be treated by the error estimates from [1]. For the k and ε transport equations, the situation is somewhat different: wall functions prescribe the generation of k , and fix ε in the near-wall cell, based on the local equilibrium considerations.

Two error estimates react differently to the wall treatment. In the momentum equation, the TSEE recognizes the high-velocity gradients in near-wall cells and reports high local errors. The MEE does not suffer from the same problem, as the wall-function modification is passed to the estimate through the modified effective viscosity on the wall boundary. Error estimation for the k and ε transport equation does not require any modification. However, the ε error estimate in the near-wall cell is invalid, as the value of ε is prescribed algebraically.

2.2.1. Systematic refinement. The solution velocity, k and ε for the coarse mesh, together with the estimated error distribution are shown in Figure 3. The error estimates highlight several regions of high error: the windward slope of the hill, the point of flow detachment on the lee slope, and the recirculation bubble. The TSEE does not pick up the high error around the detachment, as the mesh is initially too coarse to detect the peak in the $\nabla\nabla\mathbf{u}$. The MEE correctly highlights both the compression of the boundary layer and the detachment point as the regions of the high error. High errors in k are detected just downstream from the detachment point, where high shear induces high generation of k . The second region of high error is associated with the reattachment point, where ε varies rapidly. The TSEE places the error more toward the middle of the vortex, as a consequence of the inaccurate

evaluation of the second gradient close to the boundary. Error estimates for ε locate the principal error source just downstream of the detachment point (see Figure 3a) and are highlighted by both estimates.

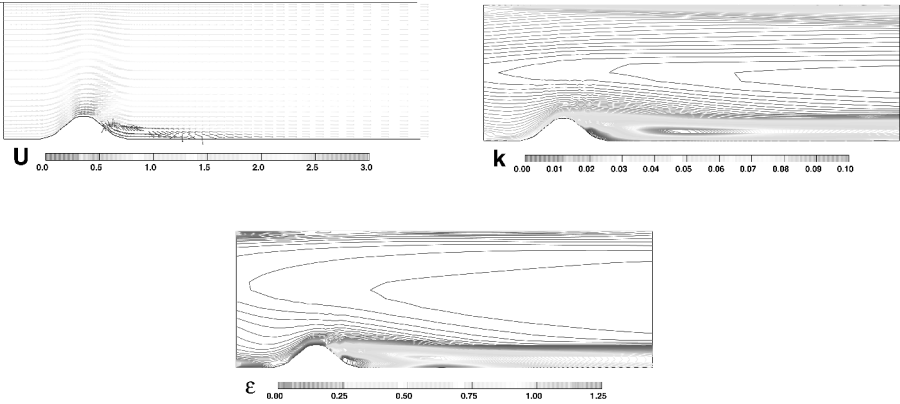
The scaling of the estimated errors with mesh refinement is given in Figure 4. After 3 levels of uniform refinement the maximum errors have typically been reduced only by about 50%. The error scaling for ε , Figure 4c, shows an increase in the maximum error with refinement. Figure 3a shows the cause of this phenomenon: the local peak in ε at the detachment point on the lee slope is resolved over a single cell even on the finest mesh, and its magnitude actually increases with better mesh resolution, thus driving the error estimate higher.

2.2.2. Adaptive error control. In the adaptive calculations, the refinement pattern is determined by combining the MEE error estimate for the velocity and k , which proved to be a good combination for turbulent incompressible flows. The y^+ for near-wall cells is prevented from dropping below 50 by explicitly excluding the affected cells from refinement parallel to the wall; it is still allowed to split the near-wall cells in a way that does not violate the y^+ condition. Having in mind that the typical error distribution in turbulent calculations contains high local error peaks, the refinement parameters are set to $\lambda_r = 1.8$, $\lambda_c = 0.2$, and $\xi = 0.6$; the results are given in Figure 5.

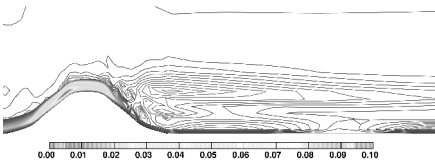
The error reduction, Figure 6, shows different behavior than for the laminar flow. The first level of refinement reduces the error magnitude, but the maximum error remains at the same place, just downstream from the summit. In the second level the error peak is moved to the near-wall cell, with only a slight change in its magnitude. This cell is consequently blocked from further refinement, based on the y^+ condition. The error reduction for k is somewhat more favorable, as it is initially possible to reduce the error without trapping the maximum error near the wall. The coarse-mesh solution shows high ε in the near-wall cell. As the refinement progresses, the peak remains in the near-wall cell, rapidly increasing in magnitude. Even after 4 levels of refinement, it is still resolved over only one cell, thus causing an increase in the maximum error.

Turbulent flows show a much larger difference between the mean and maximum error than laminar flows, opening a potential for mesh coarsening. Refinement-only and refinement with coarsening calculations are performed starting from the intermediate mesh, Figure 5b. Mesh coarsening has occurred in the center of the channel, reducing the cell count after 3 levels of refinement by approximately 20%.

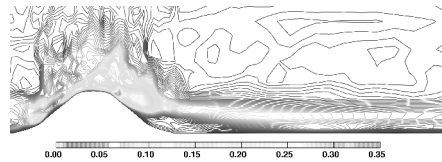
The change in mesh resolution for turbulent flows with wall functions is severely limited in near-wall cells due to the y^+ constraint. For this reason, the error scaling results for adaptive refinement in turbulent flows will be presented both with and without wall cells, Figures 6a and 6b. If near-wall cells are included, the error in velocity actually increases, as higher resolution picks up the rapid variation of \mathbf{u} around detachment, where the y^+ condition blocks further refinement. When the near-wall cells are excluded (both in uniform and adaptive refinement), adaptive refinement shows better performance. In terms of peak error reduction, the ARC shows no significant advantage over uniform refinement.



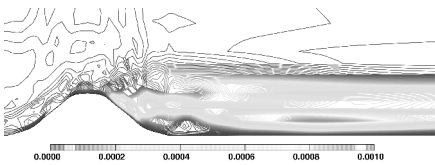
(a) Solution on the coarse uniform mesh.



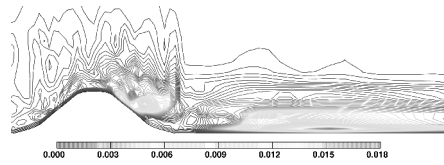
(b) Taylor series error estimate for u .



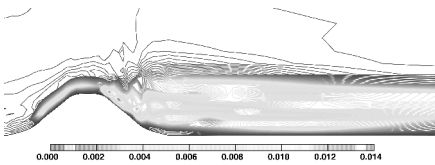
(c) Moment error estimate for u .



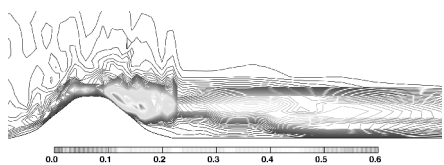
(d) Taylor series error estimate for k .



(e) Moment error estimate for k .

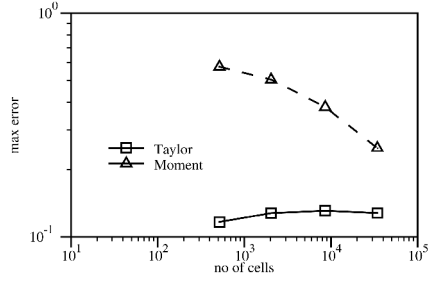
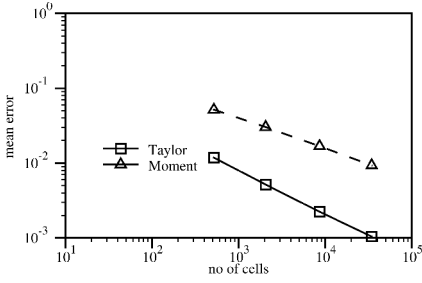


(f) Taylor series error estimate for ϵ .

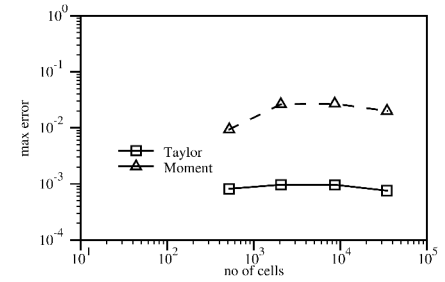
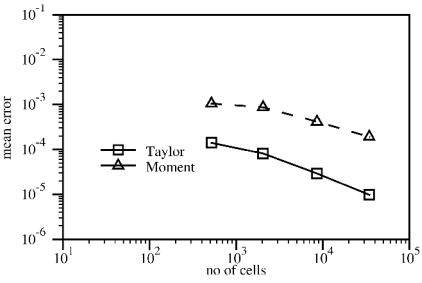


(g) Moment error estimate for ϵ .

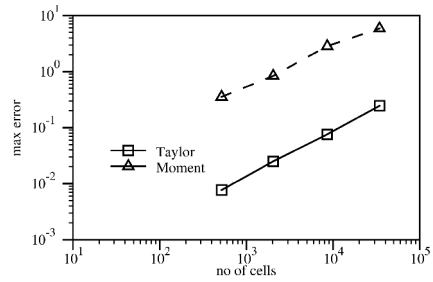
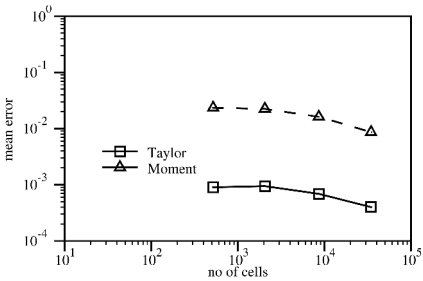
Figure 3. Turbulent flow: systematic refinement. (a) Solution on the coarse uniform mesh. (b) Taylor series error estimate for u . (c) Moment error estimate for u . (d) Taylor series error estimate for k . (e) Moment error estimate for k . (f) Taylor series error estimate for ϵ . (g) Moment error estimate for ϵ .



(a) Estimated error in u .

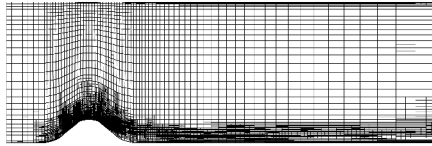
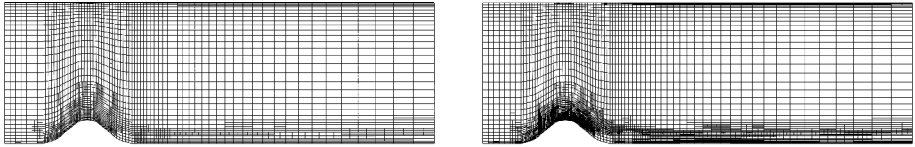


(b) Estimated error in k .

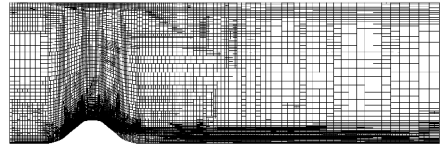
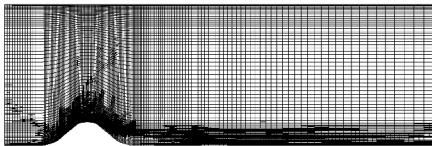


(c) Estimated error in ϵ .

Figure 4. Turbulent flow: error scaling for systematic refinement. (a) Estimated error in u . (b) Estimated error in k . (c) Estimated error in ϵ .

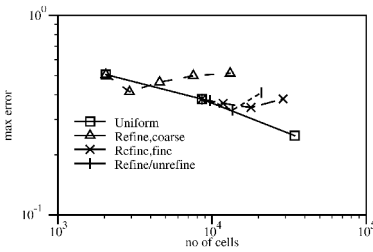


(a) Refinement starting from the coarse mesh.

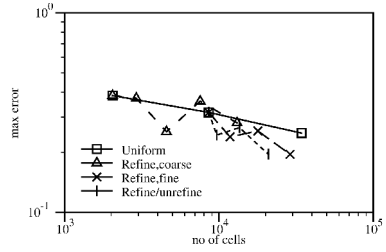


(b) Refinement-only and refinement with coarsening from intermediate mesh.

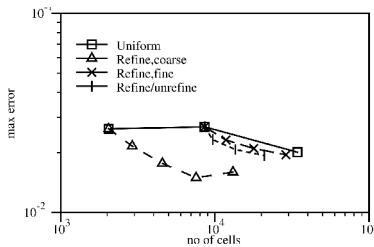
Figure 5. Turbulent flow: adaptive refinement. (a) Refinement starting from the coarse mesh. (b) Refinement-only and refinement with coarsening from intermediate mesh.



(a) Moment error estimate error for u .



(b) Moment error estimate error for u , no wall cells.



(c) Moment error estimate error scaling for k .

Figure 6. Turbulent flow: error scaling for adaptive refinement. (a) Moment error estimate error for u . (b) Moment error estimate error for u , no wall cells. (c) Moment error estimate error scaling for k .

2.3. Low-Re Calculation

The previous test case demonstrates the difficulties of mesh adaptivity in turbulent flows and registers the wall functions and high near-wall gradients as the main area of concern. An alternative to the troublesome wall functions is the integration to the wall, using a low-Re turbulence model. A variety of low-Re $k-\varepsilon$ models exists in the literature, e.g., [25–27]. As wall functions are no longer used, the error estimates can now be used without modification. The low-Re model, however, requires a very fine mesh near the wall, typically with $y^+ \approx 0.1$. The near-wall velocity field for our test case and the Launder and Sharma low-Re model [26] is shown in Figure 7.

If it were possible to decrease the high error with the use of ARC, the cost associated with low-Re models could become acceptable. For this purpose, the refinement-only procedure is used with the initial “low-Re” mesh consisting of 13,320 CVs and strong grading toward the wall. After 3 levels of refinement, the mesh consists of 38,076 CVs but, according to the error estimates, it is still too coarse. Figure 8 shows the change in the estimated maximum error with refinement. Only the final level of refinement actually decreases the error. This is, however, associated with a large increase in the number of cells, especially near the wall. The “1-irregularity” condition pushes the final cell count up to 165,470 CVs, considerably increasing the cost of the calculation. The result is still impressive: error estimates on all fields report a drop in the maximum error.

3. FLOW OVER A 3-D SWEEP STEP

This test case is included to demonstrate the performance of the ARC in three spatial dimensions. The setup consists of backward-facing step with a triangular back inside a channel [28].

The inlet velocity profile is a $1/7$ power-law profile [28] with a boundary-layer thickness of $\delta = 0.3 H$ and a free-stream velocity of 22.5 m/s with equilibrium k and ε profiles. On the top surface and the sides of the domain, a symmetry plane condition is specified.

Two uniform meshes, with 16,625 and 133,000 CVs and slight grading toward the wall, are used. The coarse-mesh solution and the estimated errors are shown in Figure 9. The iso-surface level for the estimated error is given in Table 1; the reference value is given as an indication of the typical magnitude of the variables. The highest error is located at the corner of the triangular part, particularly at the bottom of the step. Another source of error exists at the downstream edge of the triangle, where the fast side stream interacts with the vortex, as well as in the shear layer behind the step. The error estimate also highlights several detached points above the step and downstream from its corner: this error originates from the mesh skewness and nonorthogonality in regions of high local velocity gradients.

Two refinement strategies will now be used: refinement-only from the initial coarse mesh and refinement with coarsening from the fine mesh. A single level of mesh adaptation creates a mesh with 301,496 CVs, reaching the limit of the available computer resources. In order to demonstrate at least 3 levels of refinement without hitting the limit of the available computer resources, the refinement-only

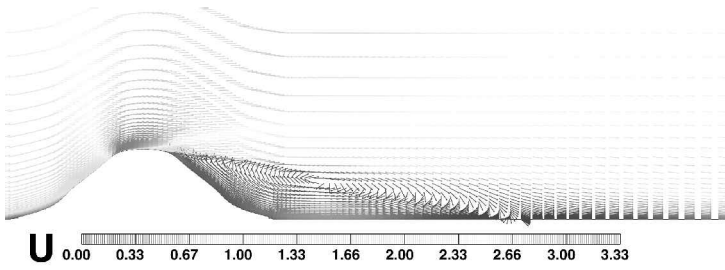
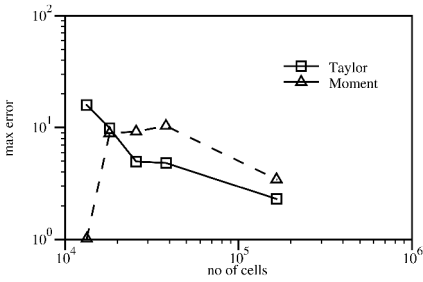
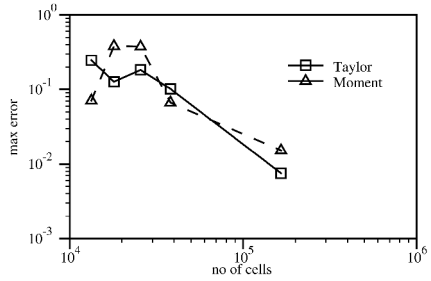


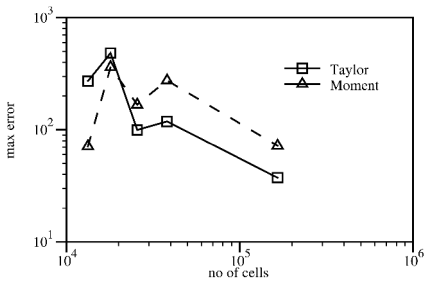
Figure 7. Turbulent flow: low-Re calculation.



(a) Maximum error in u .

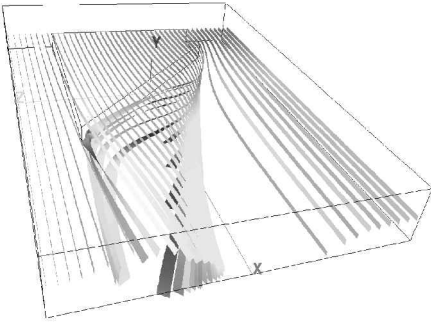


(b) Maximum error in k .



(c) Turbulent flow: error reduction with the low-Re model.

Figure 8. Turbulent flow: error reduction with the low-Re model. (a) Maximum error in u . (b) Maximum error in k . (c) Maximum error in ϵ .



(a) Stream ribbons.

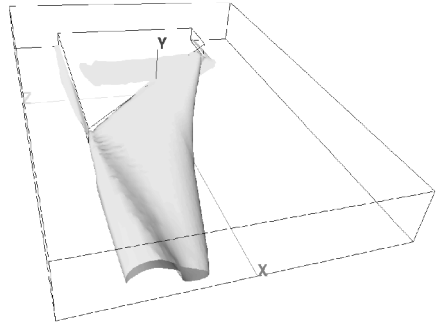
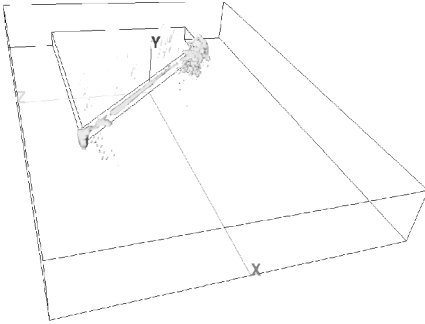
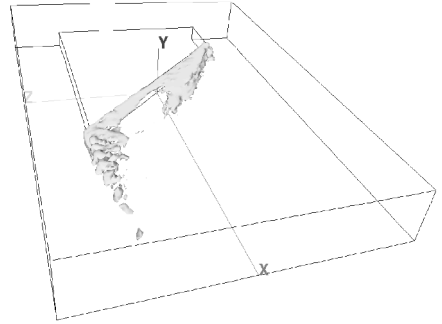
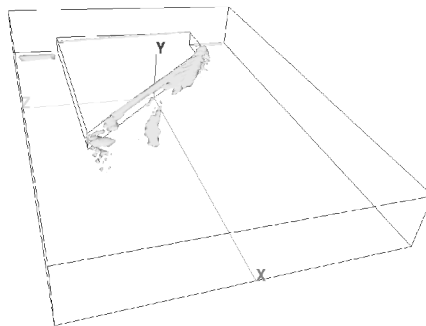
(b) Iso-surface of k .(c) Moment error estimate for \mathbf{u} .(d) Moment error estimate for k .(e) Moment error estimate for ϵ .

Figure 9. 3-D swept backward-facing step: coarse-mesh solution. (a) Stream ribbons. (b) Iso-surface of k . (c) Moment error estimate for \mathbf{u} . (d) Moment error estimate for k . (e) Moment error estimate for ϵ .

Table 1. 3-D swept backward-facing step: iso-surface level for the error estimate

Field	Reference level	Estimated max error	Error iso-surface level
\mathbf{u}	$U_0 = 22.5$ m/s	4 m/s	0.4 m/s
k	$\bar{k} = 1.5$ m ² /s ²	1.5 m ² /s ²	0.4 m ² /s ²
ε	200 m ² /s ³	150 m ² /s ³	50 m ² /s ³

calculation is performed with modified refinement parameters, Table 2. The y^+ limitation on mesh refinement is the same as above, but the initial mesh is so coarse that only one cell has been blocked from refinement during both calculations.

The refinement patterns in 3-D extend behind the step all the way along its width and are illustrated on a section around the corner in Figure 10a.

The error iso-surfaces for \mathbf{u} on the initial and refined mesh are shown in Figures 10b and 10c. Initially, the high error envelopes both corners of the triangle, also showing several points of high mesh-induced errors behind the step, and is effectively removed with the increased mesh resolution.

In terms of the maximum error reduction, neither uniform nor adaptive refinement show the expected scaling, Figure 11: both error estimates predict an increase in its magnitude as the mesh becomes finer.

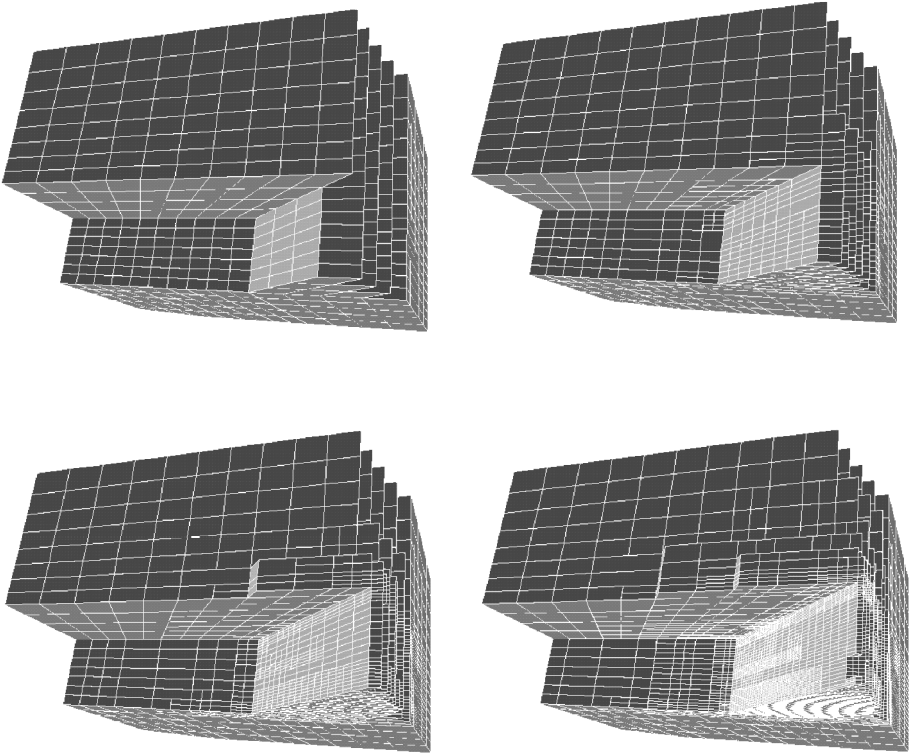
In summary, this test case shows much the same behavior as the other turbulent test case presented in this article. The error reduction is slow for both uniform and adaptive mesh refinement, with most of the problems caused by the treatment of the wall. Here, the benefit of an adaptive procedure comes more from an improvement in resolution rather than in error reduction.

4. PERFORMANCE OF ARC IN TURBULENT FLOWS

The test cases presented above allow us to draw some conclusions on the use of local mesh refinement in turbulent flow calculations. The performance of the adaptive algorithm is considerably worse than for laminar or inviscid flows [2]. The major source of difficulties is near the wall, where all fields vary very rapidly. If this region is “bridged” by the wall functions, the limits on their applicability introduce the constraint on minimum cell size. When the maximum error moves into the near-wall cell, it cannot be reduced any further. Mesh adaptivity, however, does improve the accuracy away from the wall and offers better resolution normal to the wall, which is of particular importance around the detachment and reattachment points.

Table 2. 3-D swept backward-facing step: refinement parameters

	Refinement only	Refinement and coarsening
λ_r	8.0	1.5
λ_c	—	0.5
ξ	1.2	1.2



(a) Refinement patterns.

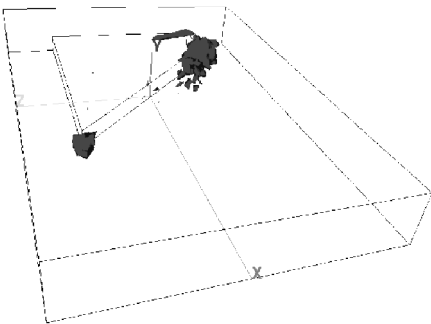
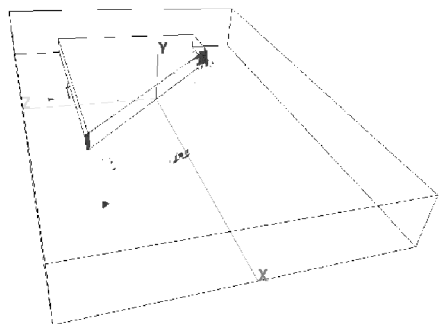
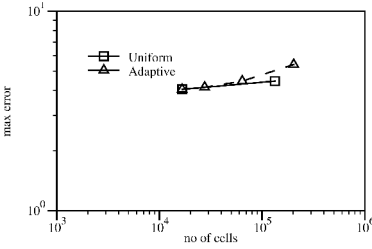
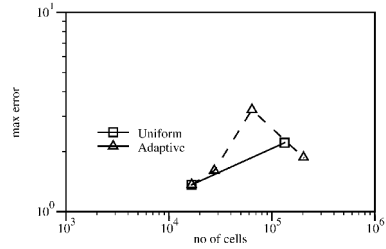
(b) Moment error estimate in \mathbf{u} iso-surface, initial mesh.(c) Moment error estimate in \mathbf{u} iso-surface, refined mesh.

Figure 10. 3-D swept backward-facing step: adaptive refinement. (a) Refinement patterns. (b) Moment error estimate in \mathbf{u} iso-surface, initial mesh. (c) Moment error estimate in \mathbf{u} iso-surface, refined mesh.



(a) Error reduction in u .



(a) Error reduction in k .

Figure 11. 3-D swept backward-facing step: scaling of the error for uniform and adaptive refinement. (a) Error reduction in u . (b). Error reduction in k .

An alternative wall treatment is the low-Re turbulence model with integration to the wall. However, this requires a considerably higher near-wall resolution, and even with an adaptive procedure, the necessary number of cells is substantially higher than for the wall-function treatment. A potential for better near-wall accuracy can possibly be found in alternative formulations of the two-equation model (e.g., the $q-\zeta$ model [29, 30]).

5. SUMMARY

This article presented some details of the adaptive local mesh refinement and coarsening procedure adopted for the automatic resolution control (ARC) algorithm [2] in conjunction with the error estimates described in [1]. In this article, we have examined the performance of the ARC in laminar and turbulent flows. The following conclusions can be drawn.

The adaptive refinement algorithm is at its best when the error caused by insufficient mesh resolution covers only a small portion of the computational domain. In this case, local refinement efficiently removes the error by augmenting mesh resolution in the affected areas. A typical example is a supersonic flow with shocks.

Laminar flows present the exact opposite of the above. The error in smoothly changing-flow is caused not only by insufficient mesh resolution, but also by insufficient mesh quality. Error estimates now perform relatively well, but local mesh refinement does not offer great gains.

Turbulent flows present a considerable challenge for local mesh adaptation. It is no longer possible to use the error estimate on only one of the fields to judge the accuracy of the solution and drive mesh refinement. This is taken into account by consulting the error estimate for more than one variable. It has been noted that the drop in the maximum error is much slower than expected, with the main source of difficulty near the wall. If this region is bridged by the wall functions, the near-wall mesh resolution is limited; if a low-Re turbulence model

is used instead, a very large number of cells is needed to resolve the high local gradients. In spite of the slow error reduction, local mesh refinement still offers some benefits, mainly through improved mesh resolution and more efficient use of the available computer resources.

Although the above conclusions are by no means final, they offer a useful guideline for the future applications of the ARC. Of particular interest is the improvement of its performance on incompressible turbulent flows, particularly in conjunction with low-Re turbulence models. Here, no limitation on the near-wall cell size is imposed, and it is expected that the mesh adaptivity will be able to provide considerable improvements in accuracy, finally reaching the ultimate goal of adaptive mesh procedures: automatically creating a solution of prescribed accuracy for the specified flow problem.

REFERENCES

1. H. Jasak and A. D. Gosman, Automatic Resolution Control for the Finite-Volume Method, Part 1: A-Posteriori Error Estimates, *Numer. Heat Transfer B*, vol. 38, no. 3, pp. 237–256, 2000.
2. H. Jasak and A. D. Gosman, Automatic Resolution Control for the Finite-Volume Method, Part 2: Adaptive Mesh Refinement, *Numer. Heat Transfer B*, vol. 38, no. 3, pp. 257–271, 2000.
3. S. Caruso, Adaptive Grid Techniques for Fluid Flow Problems, Ph.D. thesis, Thermosciences Division, Department of Mechanical Engineering, Stanford University, Stanford, CA, 1985.
4. S. Caruso, J. H. Ferziger, and J. Olinger, Adaptive Grid Techniques for Elliptic Flow Problems, Tech. Rep. TF-23, Thermosci. Div. Stanford Univ., Stanford, CA, 1985.
5. M. J. Berger and J. Olinger, Adaptive Mesh Refinement for Hyperbolic Partial Differential Equations, *J. Comput. Phys.*, vol. 53, pp. 484–512, 1984.
6. M. J. Berger and P. Collela, Local Adaptive Mesh Refinement for Shock Hydrodynamics, *J. Comput. Phys.*, vol. 82, pp. 64–84, 1989.
7. M. J. Berger and A. Jameson, Automatic Adaptive Grid Refinement for the Euler Equations, *AIAA J.*, vol. 23, no. 4, pp. 561–568, 1985.
8. J. Dompierre, M.-G. Vallet, M. Fortin, Y. Bourgault, and W. G. Habashi, Anisotropic Mesh Adaptation: Towards a Solver and User Independent CFD, AIAA Paper 97-0861, 1997.
9. A. Vidwans and Y. Kallinderis, A 3-D Finite-Volume Scheme for the Euler Equations on Adaptive Tetrahedral Grids, *J. Comput. Phys.*, vol. 113, no. 2, pp. 249–267, 1994.
10. W. Speares and E. F. Toro, A High-Resolution Algorithm for Time-Dependent Shock Dominated Problems with Adaptive Mesh Refinement, *Z. Flugwiss. Weltraumforsch.*, vol. 19, no. 4, pp. 267–281, 1995.
11. F. Moukalled and S. Acharya, A Local Adaptive Grid Procedure for Incompressible Flows with Multigridding and Equidistribution Concepts, *Int. J. Numer. Meth. Fluids*, vol. 13, no. 9, pp. 1085–1111, 1991.
12. S. S. Ochs and R. G. Rajagopalan, An Adaptively Refined Quadtree Grid Method for Incompressible Flow, *Numer. Heat Transfer B*, vol. 34, pp. 379–400, 1998.
13. J. T. Oden, W. Wu, and V. Legat, An h - p Adaptive Strategy for Finite Element Approximations of the Navier-Stokes Equations, *Int. J. Numer. Meth. Fluids*, vol. 20, pp. 831–851, 1995.

14. M. C. Thompson and J. H. Ferziger, An Adaptive Multigrid Technique for the Incompressible Navier-Stokes Equations, *J. Comput. Phys.*, vol. 82, pp. 94–121, 1989.
15. R. Vilsmeier and D. Hänel, Adaptive Methods on Unstructured Grids for Euler and Navier-Stokes Equations, *Comput. Fluids*, vol. 22, no. 4–5, pp. 485–499, 1993.
16. S. Muzafferija and D. Gosman, Finite-Volume CFD Procedure and Adaptive Error Control Strategy for Grids of Arbitrary Topology, *J. Comput. Phys.*, vol. 138, no. 2, pp. 766–787, 1997.
17. W. L. Chen, F. S. Lien, and M. Z. Leschziner, A Local Grid Refinement Scheme within a Multiblock Structured-Grid Strategy for General Flows, in *6th Int. Symp. on CFD*, Lake Tahoe, CA, Sept. 1995.
18. B. E. Launder and D. B. Spalding, The Numerical Computation of Turbulent Flows, *Comput. Meth. Appl. Mech. Eng.*, vol. 3, pp. 269–289, 1974.
19. H. G. Weller, G. Tabor, H. Jasak, and C. Fureby, A Tensorial Approach to Computational Continuum Mechanics Using Object Orientated Techniques, *Comput. Phys.*, vol. 12, no. 6, pp. 620–631, 1998.
20. R. I. Issa, Solution of the Implicitly Discretized Fluid Flow Equations by Operator-Splitting, *J. Comput. Phys.*, vol. 62, pp. 40–65, 1986.
21. H. Jasak, H. G. Weller, and A. D. Gosman, High Resolution NVD Differencing Scheme for Arbitrarily Unstructured Meshes, *Int. J. Numer. Meth. Fluids*, vol. 31, pp. 431–449, 1999.
22. T. H. Shih, W. W. Liou, A. Shabir, Z. Yang, and J. Zhu, A New $k-\varepsilon$ Eddy Viscosity Model for High Reynolds Number Turbulent Flows, NASA TM 106721, 1994.
23. G. P. Almeida, D. F. G. Durao, and M. V. Heitor, Wake Flows behind Two-Dimensional Model Hills, *Exp. Thermal Fluid Sci.*, vol. 7, pp. 87–101, 1993.
24. ERCOFTAC Workshop on Data Bases and Testing of Calculation Methods for Turbulent Flows, 4th ERCOFTAC/IAHR Workshop of Refined Flow Modelling, Karlsruhe, Germany, April 1995.
25. C. K. G. Lam and K. A. Bremhorst, Modified Form of the $k-\varepsilon$ Model for Predicting Wall Turbulence, *J. Fluids Eng.*, vol. 103, pp. 456–460, 1981.
26. B. E. Launder and B. I. Sharma, Application of the Energy-Dissipation Model of Turbulence to the Calculation of a Flow near a Spinning Disk, *Lett. Heat Mass Transfer*, vol. 1, pp. 131–138, 1974.
27. K. Y. Chien, Predictions of Channel and Boundary-Layer Flows with a Low-Reynolds-Number Turbulence Model, *AIAA J.*, vol. 20, pp. 33–38, 1982.
28. P. Moinat and M. Lesieur, Large-Eddy Simulations of Turbulent Flows over a Swept Backward-Facing Step, Tech. Rep., Laboratoire des Écoulements Géophysiques et Industriels—Institut de Mécanique de Grenoble, Grenoble, France, 1995.
29. M. M. Gibson and A. D. Dafa'Alla, Two-Equation Model for Turbulent Wall Flow, *AIAA J.*, vol. 33, no. 8, pp. 1514–1518, 1995.
30. A. D. Dafa'Alla, E. Juntasaro, and M. M. Gibson, Calculation of Oscillating Boundary Layers with the $q-\zeta$ Turbulence Model, in *3rd Int. Symp. on Engineering Turbulence Modelling and Measurements*, Crete, Greece, 1996.